Case Studies in Thermal Engineering 35 (2022) 102128

Contents lists available at ScienceDirect

Case Studies in Thermal Engineering

journal homepage: www.elsevier.com/locate/csite

Effect of the segmented fin height on the air-side performance of serrated welded spiral fin-and-tube heat exchangers

Thawatchai Keawkamrop [a], Mehrdad Mesgarpour [a], Ahmet Selim Dalkılıç [b], Ho Seon Ahn [c], Omid Mahian [d,e], Somchai Wongwises [a,f,*]

[a] Fluid Mechanics, Thermal Engineering and Multiphase Flow Research Lab (FUTURE), Department of Mechanical Engineering, Faculty of Engineering, King Mongkut's University of Technology Thonburi (KMUTT), Bangkok, 10140, Thailand
[b] Department of Mechanical Engineering, Yildiz Technical University, Yildiz, Besiktas, Istanbul, Turkey
[c] Department of Mechanical Engineering, Incheon National University, Incheon, Republic of Korea
[d] School of Chemical Engineering and Technology, Xi'an Jiaotong University, Xi'an, China
[e] Laboratory on Convective Heat and Mass Transfer, Tomsk State University, 634045, Tomsk, Russia
[f] National Science and Technology Development Agency (NSTDA), Pathum Thani, 12120, Thailand

ARTICLE INFO

Keywords:
Fin
Spiral fin
Segmented fin
Fin pitch
Heat exchanger

ABSTRACT

Serrated welded spiral fin-and-tube heat exchangers (SWSFTHXs) are experimentally investigated. The work primarily focuses on the effects of the segmented fin height (h_s) with various fin pitches (f_p) on the air-side performance (ASP). Experimental results show that SWSFTHXs provide a higher air-side heat transfer coefficient than the plain welded spiral fin-and-tube heat exchangers (PWSFTHXs) at the same f_p. The h_s has a significant effect on the Nusselt number (*Nu*) and Colburn factor (*j*), whereas f_p clearly has a greater effect on the friction factor (*f*) and Euler number (*Eu*) than h_s. Furthermore, the *Nu*, *j*, *f*, and *Eu* correlations for PWSFTHXs and SWSFTHXs are also proposed.

1. Introduction

Spiral fin-and-tube heat exchangers (SFTHXs) are basic thermal equipment that have been widely used for recovery of high-temperature flue gases. The liquid usually flows inside the tube, and the gas flows through the tube bank. Serrated welded spiral fin-and-tube heat exchangers (SWSFTHXs) are one of the most widespread geometries [1] and are used for waste heat recovery unit systems at a high temperature range. They are developed based on the plain welded spiral fin-and-tube heat exchangers (PWSFTHXs), whereby the fin tip is partially cut into narrow sections. They have been called "serrated fin" or "segmented fin." The spaced intervals on the serrated fins will disturb the boundary layers over the fin surface. Normally, SWSFTHXs give a higher average h_o [2], including higher air-side pressure drop (ΔP). The SWSFTHXs give a lower air-side heat transfer area than PWSFTHXs at the same dimensions. The fin geometry variations of SWSFTHXs have a significant effect on h_o and ΔP. However, the published experimental data about SWSFTHXs have been limited. The prior experimental research is as follows.

Kawaguchi et al. [3,4] investigated the effect of the fin height and tube arrangement of the PWSFTHXs and SWSFTHXs under the same test conditions. The experimental results indicated that the fin height had a significant effect on the heat transfer characteristics, whereby h_o increases as the fin height for the SWSFTHXs increases. SWSFTHXs also had a higher friction factor (*f*) than PWSFTHXs.

* Corresponding authorFluid Mechanics, Thermal Engineering and Multiphase Flow Research Lab (FUTURE), Department of Mechanical Engineering, Faculty of Engineering, King Mongkut's University of Technology Thonburi (KMUTT), Bangkok, 10140, Thailand.
E-mail address: somchai.won@kmutt.ac.th (S. Wongwises).

https://doi.org/10.1016/j.csite.2022.102128
Received 24 February 2022; Received in revised form 13 May 2022; Accepted 14 May 2022
Available online 21 May 2022
2214-157X/© 2022 The Authors. Published by Elsevier Ltd. This is an open access article under the CC BY license (http://creativecommons.org/licenses/by/4.0/).

Table 1
Geometrical parameter of the serrated spiral fin-and-tube heat exchangers reported in the literature.

Author	d_o (mm)	d_f (mm)	ft (mm)	f_p (mm)	w_s (mm)	h_s (mm)	Re $\times 10^{-3}$
Kawaguchi et al. [3,4]	17.3–25.4	35.3–51.3	0.9	3.3–5.0	–	2.4–6.3	5–50
Hofmann et al. [5]	38.0	68.0–78.0	0.8–1.0	3.6–3.4	4.3–4.5	–	5–30
Næss [6]	19.1–31.8	38.1–50.8	0.9	5.1	3.9	–	5–50
Ma et al. [7]	38.1	70.1	1.0	3.8–4.1	4.0	10.0	4–30
Kiatpachai et al. [17]	25.4	50.0	1.0	3.6–6.2	4.0	5.0	4–15
Zhou et al. [18]	38.0	69.8	1.0	5.1	4.0	10.9	6–12
Present work	25.4	50.0	1.2	3.6–8.4	4.0	2.5–6.5	4–19

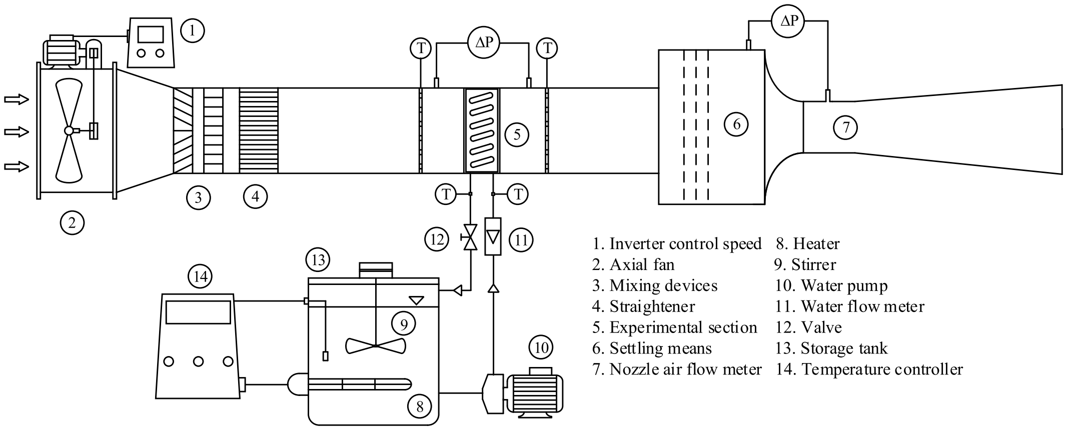

Fig. 1. Diagram of the experimental apparatus.

Table 2
Detailed geometrical parameters of the test sections.

No.	d_o (mm)	d_i (mm)	d_f (mm)	f_t (mm)	f_p (mm)	A_{fr} (mm)	P_L (mm)	P_T (mm)	w_s (mm)	h_s (mm)
1	25.40	19.86	50.0	1.20	8.47	370 × 350	68.5	66.0	4.0	–
2	25.40	19.86	50.0	1.20	5.08	370 × 350	68.5	66.0	4.0	–
3	25.40	19.86	50.0	1.20	3.63	370 × 350	68.5	66.0	4.0	–
4	25.40	19.86	50.0	1.20	8.47	370 × 350	68.5	66.0	4.0	2.5
5	25.40	19.86	50.0	1.20	5.08	370 × 350	68.5	66.0	4.0	2.5
6	25.40	19.86	50.0	1.20	3.63	370 × 350	68.5	66.0	4.0	2.5
7	25.40	19.86	50.0	1.20	8.47	370 × 350	68.5	66.0	4.0	4.5
8	25.40	19.86	50.0	1.20	5.08	370 × 350	68.5	66.0	4.0	4.5
9	25.40	19.86	50.0	1.20	3.63	370 × 350	68.5	66.0	4.0	4.5
10	25.40	19.86	51.0	1.20	8.47	370 × 350	68.5	66.0	4.0	6.5
11	25.40	19.86	51.0	1.20	5.08	370 × 350	68.5	66.0	4.0	6.5
12	25.40	19.86	51.0	1.20	3.63	370 × 350	68.5	66.0	4.0	6.5

Remark: A_{fr} = frontal area; d_f = fin outside diameter; d_i = tube inside diameter; d_o = tube outside diameter; f_t = fin thickness; h_s = segmented fin height; n_t = number of tubes per row = 5; N_{row} = number of tube rows = 2; P_L = longitudinal tube pitch; P_T = transverse tube pitch; w_s = segmented fin width; Fin material: the JISG3141 SPCC-SD (iron); Tube material: the A-179 (iron).

The tube arrangement had no large effect on the heat-transfer characteristics. Kawaguchi et al. [3,4] also proposed the correlation for predicting the Nusselt number (*Nu*) and friction factor (*f*). Hofmann et al. [5] investigated the effect of the I- and U-shaped fin geometry of SWSFTHXs on the heat transfer and pressure drop. The fin heights of the I- and U-shaped fin geometry were 15.5 and 20 mm, respectively. Test results showed that the *Nu* of the I-shaped fin geometry was greater than that of the U-shaped fin geometry for the SWSFTHXs. They proposed the *Nu* correlations. Næss et al. [6] presented the influence of tube layout and fin geometry. The experimental results showed that the equal flow areas of the transversal and diagonal planes gave the maximum *Nu*. The increasing fin pitch increased *Nu*, but it reduced the Euler number (*Eu*). The fin height was found to have an insignificant effect on the *Eu*. Ma et al. [7] studied the effect of the fin densities and tube spacing of the SWSFTHXs. The experimental results indicated that an increase in the fin density increased the *Eu*, whereas the *Nu* decreased. The large transversal tube spacing significantly reduced the *Eu*, whereas the *Nu* was unchanged. The authors predicted the *Nu* and *Eu* correlations based on the experimental data. In addition, the studies have been continuously carried out on SFTHXs (the crimped [8–11], L-footed [12–14], louver [15], and embedded and welded [16] SFTHXs), and Kiatpachai et al. [17] studied the effect of SWSFTHX fin pitches on the air-side performance (ASP). The fin pitches investigated were 3.6, 4.2, and 6.2 mm. The fin pitch had a significant effect on the ASP. The 6.2 mm fin pitch gave more dominant *f* than the other fin

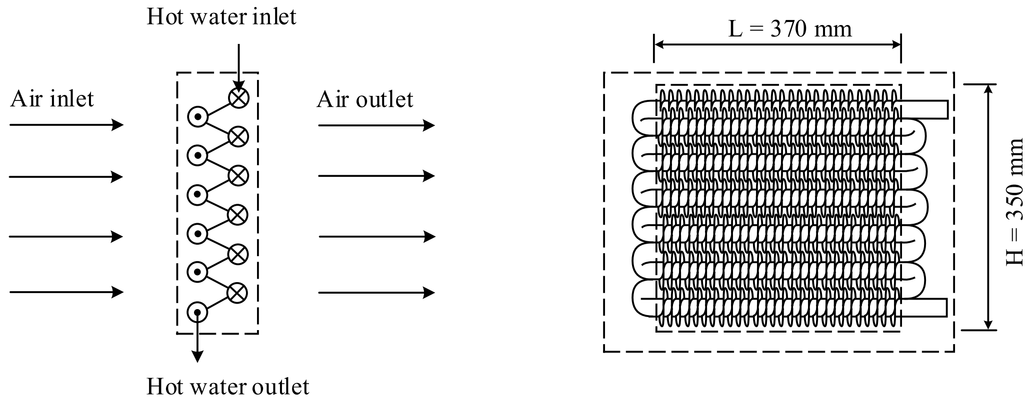

Fig. 2. Diagram of the spiral fin-and-tube heat exchangers used in the experiment.

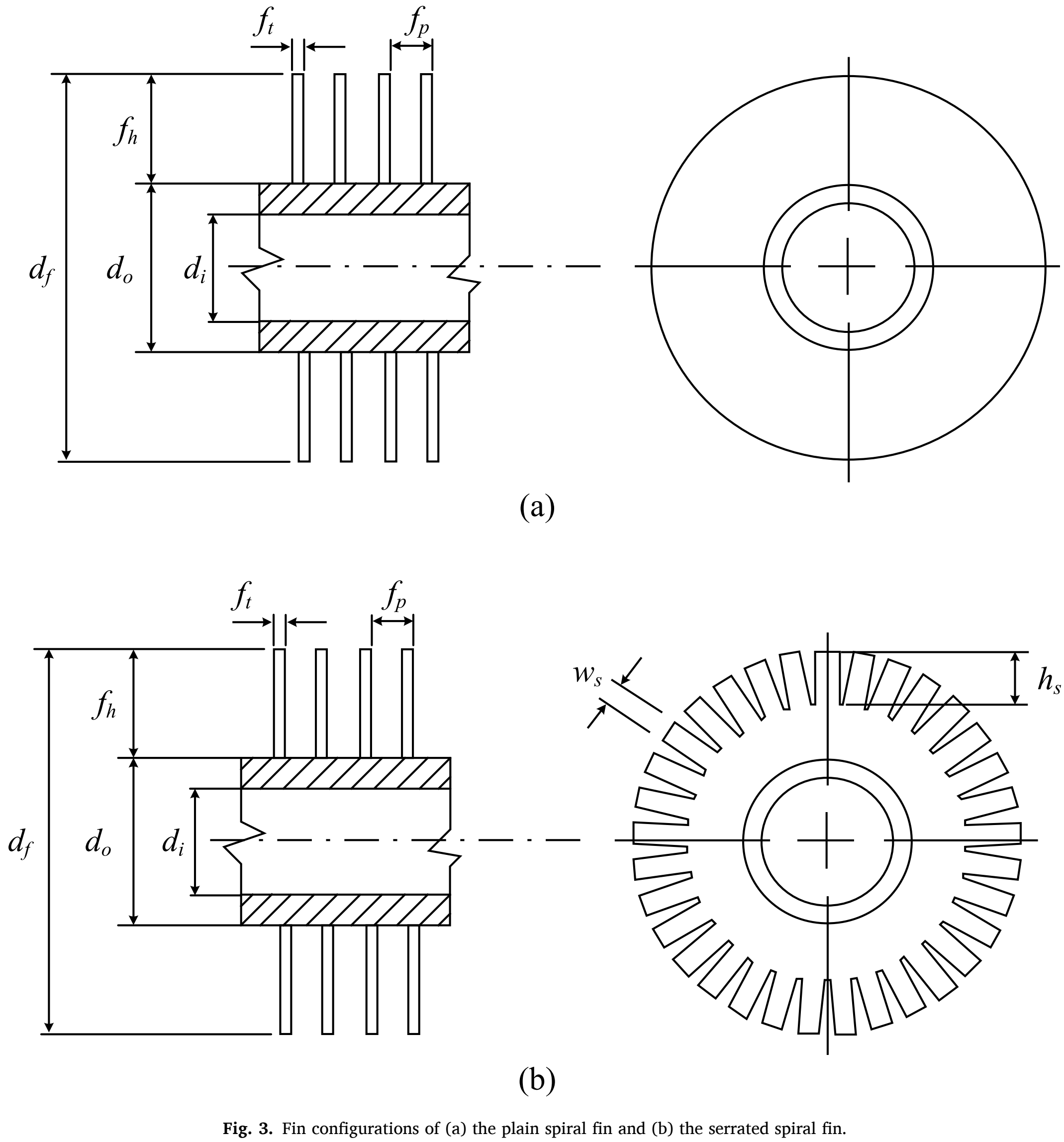

Fig. 3. Fin configurations of (a) the plain spiral fin and (b) the serrated spiral fin.

Fig. 4. The tested plain welded spiral fin-and-tube heat exchanger (left) and serrated welded spiral fin-and-tube heat exchanger (right).

Table 3
Test conditions.

Parameter	Condition
$T_{a,in}$, °C	31.5 ± 0.5
$T_{w,in}$, °C	60, 65, and 70
$\dot{V}_w$, LPM	12 and 14
V_{fr}, m/s	1.5–7.1

Remark: $T_{a,in}$ = inlet air dry bulb temperature; $\dot{V}_w$ = water volume flow rate.

pitch. They also proposed the Colburn factor (j) and f correlations. Furthermore, Zhou et al. [18] studied the effect of a twist of the fin on the performance of the SWSFTHXs. The experiment was done at Reynolds numbers between 6,000 and 12,000. The top of the segmented fin was compared between the serrated fin and twisting serrated fin, for which the torsion angle and deflection angle were 27°–30° and 5°–10°, respectively. The twisting of the segmented fin led to a significant increase in the *Nu* and *Eu*. Moreover, optimization techniques have been applied in the design of some types of finned heat exchangers such as the cross-flow plate-fin heat exchanger [19,20].

Table 1 summarizes the relevant experimental works on the SWSFTHXs [3–7,17,18]. Even though these studies reported the effect of geometric parameters on the ASP, there remains room for further experimental research. According to the literature review, the influence of the fin segment has not been seriously studied in an experiment. Therefore, the main purpose of this study is to investigate the effect of h_s with various fin pitches (f_p) of the SWSFTHXs on the ASP.

2. Experimental apparatus and procedure

The apparatus of Keawkamrop et al. [11] was used in the experiment. A schematic diagram can be seen in Fig. 1. Table 2 shows the test sections with the 12-fin configurations and a detailed geometric parameter. The outside diameter of a fin is a couple of fin heights

Table 4
Measurement accuracies.

Parameter	Accuracy
Air-side thermocouple probes	$\pm0.1\ ^{\circ}C$
Water-side thermocouple probes	$\pm0.1\ ^{\circ}C$
Water flow meter	±0.4 (±0.02 of full scale) *LPM*
Digital manometer	±0.5 Pa

Table 5
Uncertainties of the parameters.

Parameter	Maximum uncertainties (%)
$\dot{Q}_a$	±6.50
$\dot{Q}_w$	±12.13
V_{fr}	±1.77
Re_{do}	±1.89
ΔP	±5.41
h_o	±9.11
j	±9.18
f	±6.23

(f_h) plus the tube outside diameter. The h_s and f_p are maximum values that can be produced by the tube finning machine. The width of the segmented fin is the standard value that could be produced from the tube finning machine. The test sections consist of the PWSFTHXs (Nos. 1–3) and SWSFTHXs (Nos. 4–12). The size of the frontal area of all test sections is 370 × 350 mm, as shown in Fig. 2. The tube circuits are arranged in a Z shape, which is a combination of the muti-pass parallel and counter cross-flow with two tube rows. The SWSFTHXs have three different h_s and f_p values. The PWSFTHXs have three f_p values, for which the schematic diagram is shown in Fig. 3. The h_s values investigated are 2.50, 4.50, and 6.50 mm. The f_p values are 3.63 (7 fpi), 5.08 (5 fpi), and 8.47 (3 fpi) mm. The tested PWSFTHXs and SWSFTHXs can be seen in Fig. 4. Table 3 shows the experimental conditions. The inlet frontal air velocities cover the velocities used in the industry, as reported by Xie et al. [21]. The inlet air temperature is the ambient temperature. The inlet water temperatures are set to achieve the maximum temperature difference between inlet and outlet water. The water flow rates corresponding to turbulent flow are used in the experiment. The data are recorded at steady-state condition. The energy imbalance, which is obtained from the heat transfer rate between both sides, is limited to no more than 0.05, which follows the ANSI/ASHRAE 33 standards [22]. The measurement accuracies and experimental uncertainties are shown in Tables 4 and 5, respectively.

3. Data reduction

The j and Nu, which are transformed from the air-side heat transfer coefficient (h_o), are key to investigating the ASP of the SWSFTHXs.

The total thermal resistance of the PWSFTHXs and SWSFTHXs consists of the conduction resistance and convection resistance, as follows:

$$\frac{1}{UA}=\frac{1}{h_iA_i}+\frac{\ln(d_o/d_i)}{2\pi k_t L}+\frac{1}{\eta_o h_o A_o} \tag{1}$$

The UA is determined from the number of transfer units (NTU)

$$UA=C_{\min}(NTU) \tag{2}$$

The NTU is calculated based on the Engineering Science Data Unit [23] and Taborek [24], as in Eqs. (3) and (4).

The effectiveness of the multi-pass parallel cross-flow for $N_{row}=2$ is

$$\varepsilon_p=\left(1-\frac{K}{2}\right)\left(1-e^{-2K/C_A^*}\right),\ K=1-e^{-NTU_A/\left(C_A^*/2\right)} \tag{3}$$

and the effectiveness of the multi-pass counter cross-flow for $N_{row}=2$ is

$$\varepsilon_c=1-\left[\frac{K}{2}+\left(1-\frac{K}{2}\right)e^{2K/C_A^*}\right]^{-1},\ K=1-e^{-NTU_A/\left(C_A^*/2\right)} \tag{4}$$

in which air-side (specified as Fluid A) is mixed and water-side (specified as Fluid B) is unmixed.

The minimum heat capacity rate ($C_{\min}$) in this study is obtained from Fluid A.

$$C_A^*=C_{\min}/C_{\max} \tag{5}$$

where

$$C_{\min} = \dot{m}_a C_{p,a} \tag{6}$$

and

$$C_{\max} = \dot{m}_w C_{p,w} \tag{7}$$

The average effectiveness, as shown in Eq. (8), is calculated from

$$\varepsilon_A = \frac{\varepsilon_p + \varepsilon_c}{2} \tag{8}$$

The average heat-transfer rate is calculated from

$$\dot{Q}_{ave} = \frac{|\dot{Q}_a| + |\dot{Q}_w|}{2} \tag{9}$$

where

$$\dot{Q}_a = \dot{m}_a C_{p,a}\left(T_{a,out} - T_{a,in}\right) \tag{10}$$

and

$$\dot{Q}_w = \dot{m}_w C_{p,w}\left(T_{w,in} - T_{w,out}\right) \tag{11}$$

The effectiveness is calculated from

$$\varepsilon = \frac{\dot{Q}_{ave}}{\dot{Q}_{\max}} \tag{12}$$

where

$$\dot{Q}_{\max} = C_{\min}\left(T_{h,in} - T_{c,in}\right) \tag{13}$$

The tube-side heat-transfer coefficient is determined using Gnielinski equation [25].

$$h_i = \left(\frac{k_w}{d_i}\right)\frac{(\mathrm{Re}_{di} - 1000)\mathrm{Pr}(f_i/2)}{1 + 12.7\sqrt{f_i/2}\left(\mathrm{Pr}^{2/3} - 1\right)} \tag{14}$$

where $2300 < Re_{di} < 5 \times 10^6$; $0.5 \leq Pr \leq 2000$.

And

$$f_i = (1.58\ln\mathrm{Re}_{di} - 3.28)^{-2} \tag{15}$$

The Reynolds number (Re_{di}) is calculated from

$$Re_{di} = \rho_w V_i d_i / \mu_w \tag{16}$$

The fin efficiency (η_f) can be calculated from

$$\eta_f = 1 + \frac{A_o}{A_f}(\eta_o - 1) \tag{17}$$

where the overall surface effectiveness (η_o) is

$$\eta_o = \frac{1}{h_o A_o\left[\frac{1}{UA} - \frac{1}{h_i A_i} - \frac{\ln(d_o/d_i)}{2\pi k_t L}\right]} \tag{18}$$

The η_f proposed by Gardner [26] is determined from

$$\eta_f = \frac{2\psi}{\varphi(1+\psi)}\frac{I_1(\varphi R_o)K_1(\varphi R_i) - I_1(\varphi R_i)K_1(\varphi R_o)}{I_0(\varphi R_i)K_1(\varphi R_o) + I_1(\varphi R_o)K_0(\varphi R_i)} \tag{19}$$

where

$$\varphi = (r_o - r_i)^{3/2}\sqrt{\frac{2h_o}{k_f A_p}} \tag{20}$$

and

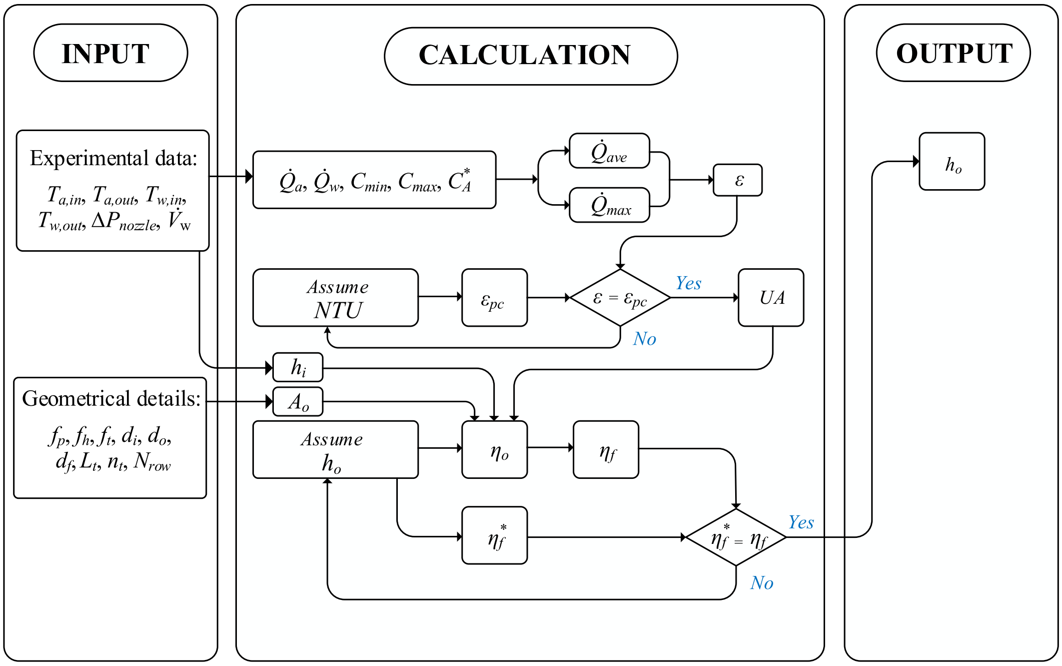

Fig. 5. Computation of the air side heat transfer coefficient.

$$\psi = r_i / r_o \tag{21}$$

where I_0, I_1 and K_0, K_1 are the modified Bessel function solution of the first kind, and second kind, respectively; r_o is the external radius of the fin; r_i is the internal radius of the fin; φ is the combination of terms; and ψ is the radius ratio.

The flowchart for the computation of h_o is presented in Fig. 5. The ASP is interpreted in terms of dimensionless j, Nu, f, and Eu.

$$j = \frac{Nu}{\mathrm{Re}_{do}\mathrm{Pr}^{1/3}} = \frac{h_o}{\rho_a V_{\max} c_p}(\mathrm{Pr})^{2/3} \tag{22}$$

The f is proposed by Key and London [27] as follows:

$$f = \left(\frac{A_{\min}}{A_o}\right)\left(\frac{\rho_m}{\rho_1}\right)\left[\frac{2\Delta P \rho_1}{G_c^2} - \left(1+\sigma^2\right)\left(\frac{\rho_1}{\rho_2} - 1\right)\right] \tag{23}$$

where $A_{\min}$ is the minimum free-flow area; A_o is the total heat-transfer area; G_c is the air mass flux based on the $A_{\min}$; ρ_1, ρ_2 and ρ_m are density of air at inlet and out let, and average air density, respectively; and σ is the ratio of the minimum free-flow area to the frontal area.

The pressure loss coefficient per tube row passed (Euler number; Eu) [6] is calculated from

$$Eu = \frac{2\Delta P \rho_m}{N_{row} G_c^2} \tag{24}$$

The following sentences are added into the manuscript.

The maximum uncertainties of the j and f calculated from the root mean sum square method are 9.18% and 6.23%, respectively. The uncertainty increases as the Reynolds number decreases.

4. Results and discussion

Fig. 6 shows comparisons between the average heat transfer rate ($\dot{Q}_{ave}$), air-side heat transfer coefficient (h_o), and air-side pressure drop (ΔP) obtained from the PWSFTHXs and those obtained from SWSFTHXs at a fixed inlet water temperature ($T_{w,in}$) of 60 °C and an inlet water mass flow rate ($\dot{m}_{w,in}$) of 0.20 kg/s. They are plotted against the frontal air velocity (V_{fr}), which is between 2 and 7 m/s. As expected, the experimental results show $\dot{Q}_{ave}$, h_o, and ΔP increase with increasing V_{fr}. The $\dot{Q}_{ave}$ of the PWSFTHXs and SWSFTHXs tends to be in the same direction. The $\dot{Q}_{ave}$ obtained from the SWSFTHXs is higher than that of the PWSFTHXs. An h_s of 6.50 mm for SWSFTHXs provides the highest $\dot{Q}_{ave}$ at all f_p values. A f_p of 8.47 mm gives the lowest $\dot{Q}_{ave}$. This is because the larger f_p generally reduces the air-side area, which leads to a decrease in the $\dot{Q}_{ave}$. The effects of f_p and h_s on h_o can be seen in Fig. 6 (b). The experimental results also indicate that the SWSFTHXs clearly have a higher h_o than the PWSFTHXs by about 15.8–20.5%, based on the same V_{fr}. It is clear

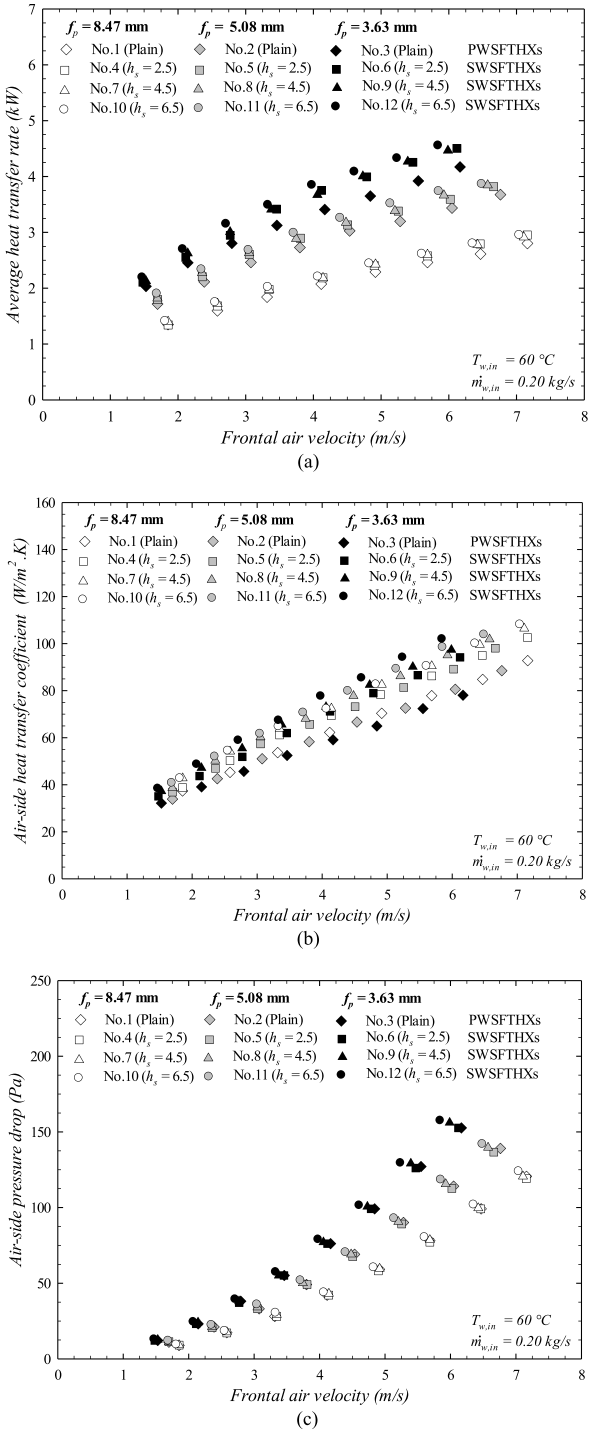

Fig. 6. Effect of fin pitch and segmented fin height on (a) the average heat-transfer rate, (b) the air-side heat transfer coefficient, and (c) the air-side pressure drop.

that the spaced interval of the serrated fins has a significant effect on h_o. This is because the presence of serrations will disturb the function of boundary layers over the fin surface, leading to a better h_o. The effects of f_p and h_s on the ΔP can be seen in Fig. 6 (c). The ΔP increases with decreasing f_p, whereas h_s increases. The ΔP with a f_p of 3.63 and 5.08 mm is higher than that of 8.47 mm by about 43.0–101.6% and 32.9–75.0%, respectively, with the same V_{fr}. This is because a decrease of f_p increases the blocking of the flow area, which leads to a significant increase in ΔP. It seems the SWSFTHXs give a higher ΔP than the PWSFTHXs. The ΔP from an h_s of 6.5 mm is higher than the other h_s because of higher turbulence caused by segmented fins.

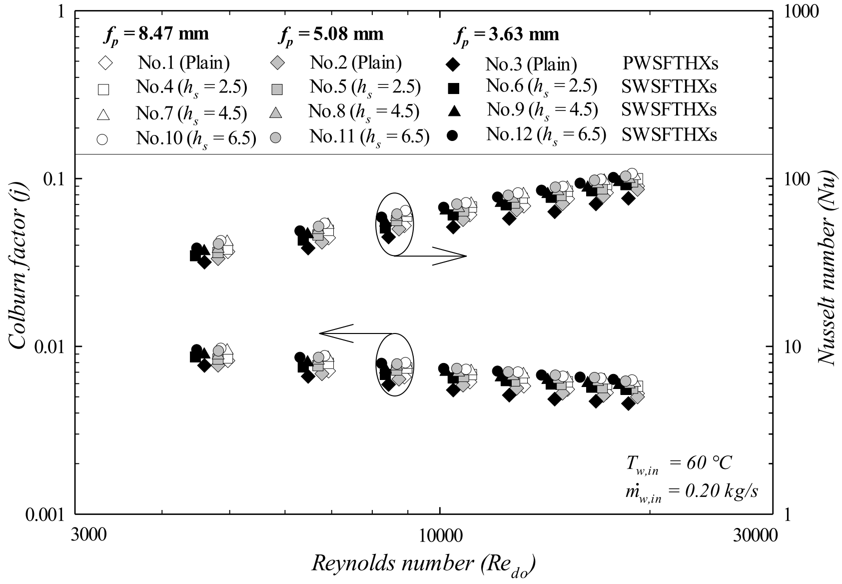

(a)

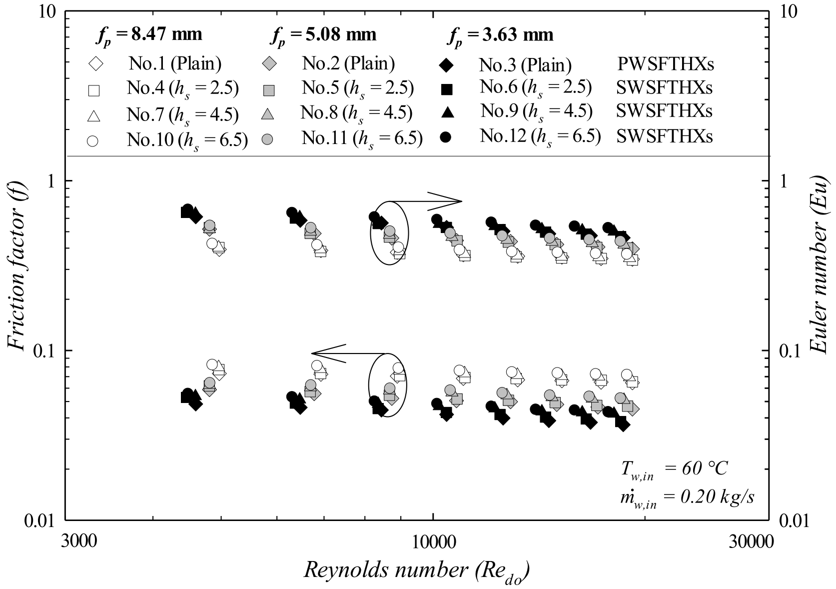

(b)

Fig. 7. Effect of fin pitch and segmented fin height on (a) the Nusselt number and Colburn factor, and (b) the friction factor and Euler number with different Reynolds numbers.

The effect of f_p and h_s on the Nu, j, f, and Eu for different Reynolds numbers (Re_{do}) is shown in Fig. 7. Fig. 7(a) shows the comparison between the Nu and j, whereas Fig. 7(b) shows the comparison between the f and Eu. The experimental results show Nu increases with an increase in Re_{do}, which is the opposite of the plots of the j, f, and Eu. Additionally, f_p and h_s affect the heat transfer (j, Nu) and pressure drop characteristic (f, Eu) in the same direction.

Fig. 8(a–c) shows the variations of j and f with Re_{do} for the different $T_{w,in}$ and $\dot{m}_{w,in}$ values. The results indicate that the j and f are similar in magnitude and trend. As expected, the PWSFTHXs have lower j than the SWSFTHXs. This is because the SWSFTHXs have better air mixing, which results in higher heat transfer enhancement [17]. The results also show h_s has a significant effect on j. The effect of f_p also corresponds with Kiatpachai et al.'s findings [17]. The SWSFTHXs provide a higher f than the PWSFTHXs, whereby the SWSFTHXs with an h_s of 6.5 mm give a higher f than the other h_s for all f_p values. Experimental results also show the effect of f_p is clearly observable compared to that of h_s. A f_p of 8.47 mm gives a greater f than other f_p values. This is because $A_{\min}/A_o$ in Eq. (23) increases when f_p increases, which results in an increase of f.

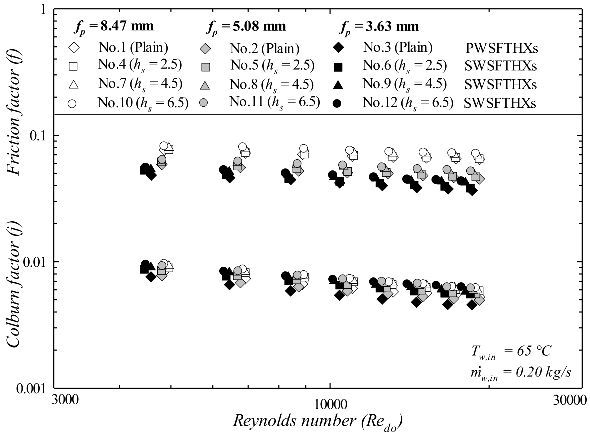

(a)

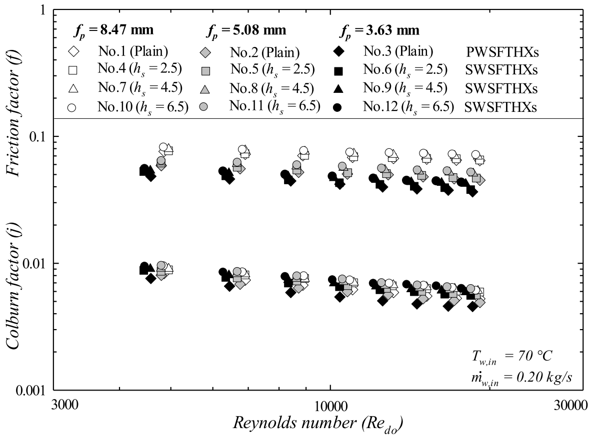

(b)

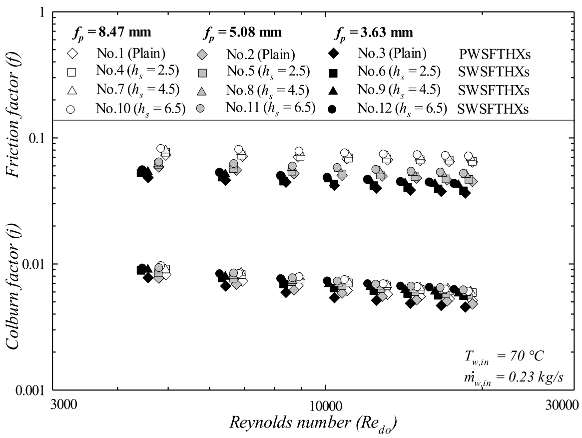

(c)

Fig. 8. Effect of fin pitch and segmented fin height on the Colburn factor and friction factor at (a) $T_{w,in} = 65\ ^\circ\text{C}/\dot{m}_{w,in} = 0.20$ kg/s, (b) $T_{w,in} = 70\ ^\circ\text{C}/\dot{m}_{w,in} = 0.20$ kg/s, and (c) $T_{w,in} = 70\ ^\circ\text{C}/\dot{m}_{w,in} = 0.23$ kg/s.

The corresponding correlations for the PWSFTHXs and SWSFTHXs are developed based on the basic correlation, as suggested by Wang et al. [28]. Test results indicate f_p is the dominant parameter on the frictional characteristics. Consequently, the f_p/d_0 which is a dimensionless parameter are therefore added to the f and Eu, as reported by Pongsoi et al. [9].

The proposed Nu, j, f, and Eu correlations are as follows:

$$Nu_{corr} = 0.1172\text{Re}_{do}^{0.68095} \tag{25}$$

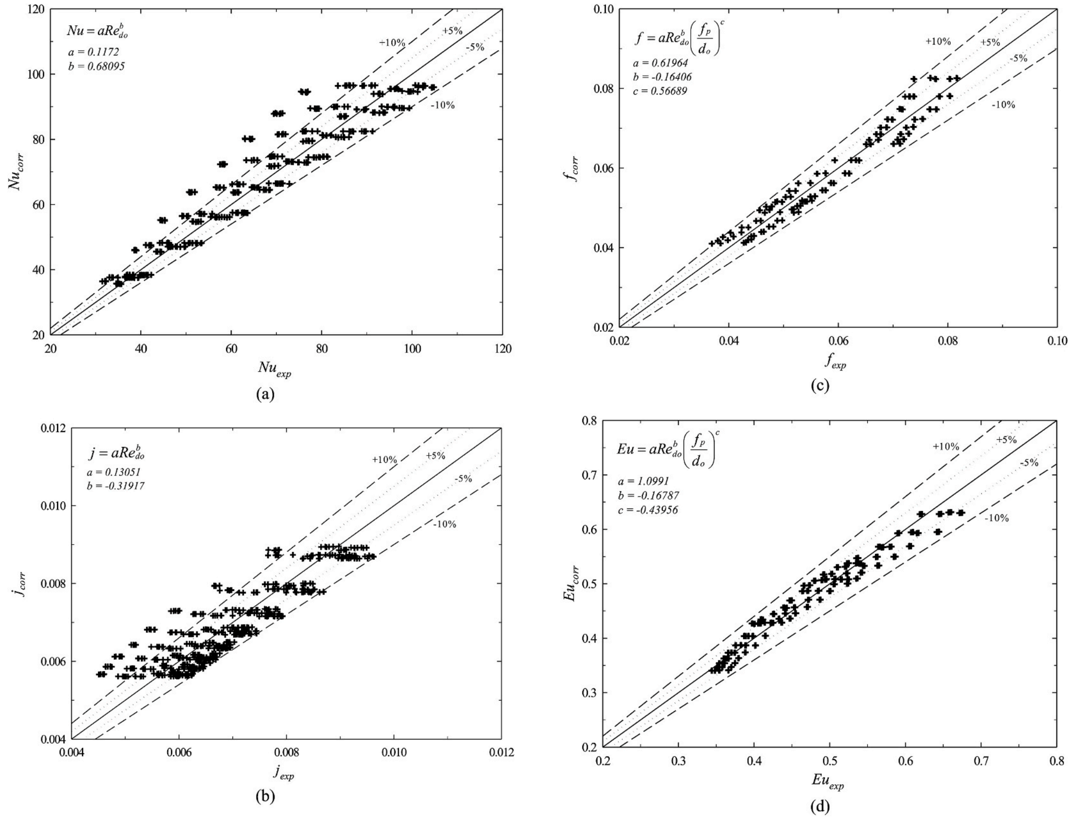

Fig. 9. Measured versus predicted parameters: (a) Nusselt number, (b) Colburn factor, (c) friction factor, and (d) Euler number.

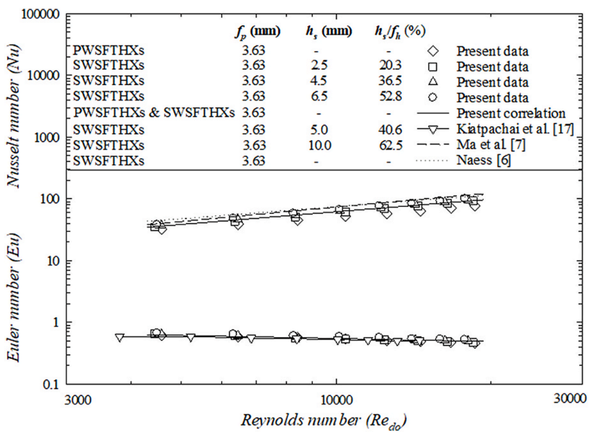

Fig. 10. Comparison between present experimental data and correlations.

$$j_{corr} = 0.13051\mathrm{Re}_{do}^{-0.31917} \tag{26}$$

$$f_{corr} = 0.61964\mathrm{Re}_{do}^{-0.16406}\left(\frac{f_p}{d_o}\right)^{0.56689} \tag{27}$$

$$Eu_{corr} = 1.0991\mathrm{Re}_{do}^{-0.16787}\left(\frac{f_p}{d_o}\right)^{-0.43956} \tag{28}$$

where $4000 < Re_{do} < 19000$ and $Pr = 0.727$

$$Mean\ deviation\ = \frac{1}{M}\left[\sum_{1}^{M}\frac{|\Phi_{corr} - \Phi_{\exp}|}{\Phi_{\exp}}\right] \times 100\% \tag{29}$$

The mean deviations for the Nu, j, f, and Eu correlations are 7.22, 7.21, 4.46, and 2.96%, respectively. Fig. 9(a–d) compares the results from correlations and with the experimental data. The ASP correlations proposed (Eq. (25), (26), (27), and (28)) can describe the ASP well as 83.85, 84.54, 99.48, and 100% of Nu, j, f, and Eu within ±10%, respectively. Fig. 10 compares the ASP in terms of the Nu and Eu of the PWSFTHXs and SWSFTHXs. The ratio of h_s and f_h is determined for comparison with the results obtained from previous studies. The h_s/f_h ratio in this study is between 20.3 and 52.8%, which increases as h_s increases. The results correspond with the data of Naess et al. [6], Ma et al. [7], and Kiatpachai et al. [17], in which the ΔP is presented in the terms of Eu. The trend of Nu and Eu is similar to that found in the current study. The Nu increases with increasing Re_{do}, whereas the Eu decreases with increasing Re_{do}. The heat exchanger with a h_s/f_h ratio of 62.5% [7] gives a higher Nu than the h_s/f_h ratio in the present study. The Eu calculated from the ΔP, as reported by Kiatpachai et al. [17] ($h_s/f_h = 40.6\%$), corresponds with the Eu calculated from the present data ($h_s/f_h = 20.3$, 36.5, 52.8%).

5. Conclusion

The experimental results can be concluded as follows:

- The average heat transfer rate ($\dot{Q}_{ave}$), air-side heat transfer coefficient (h_o), and air-side pressure drop (ΔP) increase with increasing frontal air velocity (V_{fr}).
- The $\dot{Q}_{ave}$ and ΔP increase as the fin pitch (f_p) decreases and the segmented fin height (h_s) increases.
- An h_s of 6.50 mm for serrated welded spiral fin-and-tube heat exchangers (SWSFTHXs) has the highest $\dot{Q}_{ave}$ out of all the f_p values.
- The SWSFTHXs give a higher h_O than the plain welded spiral fin-and-tube heat exchangers (PWSFTHXs).
- The ΔP increases with decreasing f_p and with increasing h_s.
- The h_s has a significant effect on Nu and j.
- The f_p has a clearer effect on f and Eu than h_s.
- The Nu, j, f, and Eu correlations for the PWSFTHXs and SWSFTHXs are developed.

Author statement

Thawatchai Keawkamrop: Carried out the experiment, Writing-Original draft preparation. Mehrdad Mesgarpour: Investigation. Ahmet Selim Dalkılıç: Investigation. Ho Seon Ahn: Investigation. Omid Mahian: Investigation. Somchai Wongwises: Supervision, Writing-Reviewing and Editing.

Declaration of competing interest

The authors declare that they have no known competing financial interests or personal relationships that could have appeared to influence the work reported in this paper.

Acknowledgments

The first author acknowledges the Royal Golden Jubilee Ph.D. Program. The second author acknowledges the KMUTT Postdoctoral Fellowship. The third, fourth and fifth authors acknowledge the KMUTT Visiting Professorships. The fifth author would like to thank the support of Tomsk State University Development Programme (Priority-2030) for this research. The sixth author acknowledges the NSTDA Research Chair Grant, and the Thailand Science Research and Innovation for the Fundamental Fund 2022.

References

[1] A. Lemouedda, A. Schmid, E. Franz, M. Breuer, A. Delgado, Numerical investigations for the optimization of serrated finned-tube heat exchangers, Appl. Therm. Eng. 31 (8–9) (2011) 1393–1401.
[2] C.T. Ó Cléirigh, W.J. Smith, Can CFD accurately predict the heat-transfer and pressure-drop performance of finned-tube bundles? Appl. Therm. Eng. 73 (1) (2014) 681–690.
[3] K. Kawaguchi, K. Okui, T. Kashi, The heat transfer and pressure drop characteristics of finned tube banks in forced convection (comparison of the pressure drop characteristics of spiral fins and serrated fins), Heat Tran. Asian Res. 33 (7) (2004) 431–444.

[4] K. Kawaguchi, K. Okui, T. Asai, Y. Hasegawa, The heat transfer and pressure drop characteristics of the finned tube banks in forced convection (effects of fin height on heat transfer characteristics), Heat Tran. Asian Res. 35 (3) (2006) 194–208.
[5] R. Hofmann, F. Frasz, K. Ponweiser, Heat transfer and pressure drop performance comparison of finned-tube bundles in forced convection, WSEAS Trans. Heat Mass Transf. 2 (4) (2008) 72–88.
[6] E. Næss, Experimental investigation of heat transfer and pressure drop in serrated-fin tube bundles with staggered tube layouts, Int. J. Heat Mass Tran. 30 (13) (2010) 1531–1537.
[7] Y. Ma, Y. Yuan, Y. Liu, X. Hu, Y. Huang, Experimental investigation of heat transfer and pressure drop in serrated finned tube banks with staggered layouts, Appl. Therm. Eng. 37 (2012) 314–323.
[8] P. Pongsoi, S. Pikulkajorn, C.C. Wang, S. Wongwises, Effect of fin pitches on the air-side performance of crimped spiral fin-and-tube heat exchangers with a multipass parallel and counter cross-flow configuration, Int. J. Heat Mass Tran. 54 (9–10) (2011) 2234–2240.
[9] P. Pongsoi, S. Pikulkajorn, C.C. Wang, S. Wongwises, Effect of number of tube rows on the air-side performance of crimped spiral fin-and-tube heat exchangers with a multipass parallel and counter cross-flow configuration, Int. J. Heat Mass Tran. 55 (4) (2012) 1403–1411.
[10] P. Pongsoi, S. Pikulkajorn, S. Wongwises, Effect of fin pitches on the optimum heat transfer performance of crimped spiral fin-and-tube heat exchangers, Int. J. Heat Mass Tran. 55 (23–24) (2012) 6555–6566.
[11] T. Keawkamrop, L.G. Asirvatham, A.S. Dalkılıç, H.S. Ahn, O. Mahian, S. Wongwises, An experimental investigation of the air-side performance of crimped spiral fin-and-tube heat exchangers with a small tube diameter, Int. J. Heat Mass Tran. 178 (2021), 121571.
[12] P. Pongsoi, S. Pikulkajorn, S. Wongwises, Experimental study on the air-side performance of a multipass parallel and counter cross-flow L-footed spiral fin-and-tube heat exchanger, Heat Tran. Eng. 33 (15) (2012) 1–13.
[13] P. Pongsoi, P. Promoppatum, S. Pikulkajorn, S. Wongwises, Effect of fin pitches on the air-side performance of L-footed spiral fin-and-tube heat exchangers, Int. J. Heat Mass Tran. 59 (2013) 75–82.
[14] P. Pongsoi, S. Wongwises, Determination of fin pitches for maximum performance index of L-footed spiral fin-and-tube heat exchangers, J. Therm. Eng. 1 (1) (2015) 251–262.
[15] P. Kiatpachai, T. Keawkamrop, L.G. Asirvatham, M. Mesgarpour, A.S. Dalkılıç, H.S. Ahn, O. Mahian, S. Wongwises, An experimental study of the air-side performance of a novel louver spiral fin-and-tube heat exchanger, Alex. Eng. J. 61 (12) (2022) 9811–9818.
[16] P. Kiatpachai, T. Kaewkamrop, M. Mesgarpour, H.S. Ahn, A.S. Dalkılıç, O. Mahian, S. Wongwises, Air-side performance of embedded and welded spiral fin and tube heat exchangers, Case Stud. Therm. Eng. 30 (2022), 101721.
[17] P. Kiatpachai, S. Pikulkajorn, S. Wongwises, Air-side performance of serrated welded spiral fin-and-tube heat exchangers, Int. J. Heat Mass Tran. 89 (2015) 724–732.
[18] H. Zhou, D. Liu, Q. Sheng, M. Hu, Y. Cheng, K. Cen, Research on gas side performance of staggered fin-tube bundles with different serrated fin geometries, Int. J. Heat Mass Tran. 152 (2020), 119509.
[19] D.B. Raja, R.L. Jhala, V. Patel, Many-objective optimization of cross-flow plate-fin heat exchanger, Int. J. Therm. Sci. 118 (2017) 320–339.
[20] B.D. Raja, R.L. Jhala, V. Patel, Thermal design and optimization of fin-and-tube heat exchanger using heat transfer search algorithm, Therm. Sci. Eng. Prog. 4 (2017) 45–57.
[21] G. Xie, Q. Wang, B. Sunden, Parametric study and multiple correlations on air-side heat transfer and friction characteristics of fin-and-tube heat exchangers with large number of large-diameter tube rows, Appl. Therm. Eng. 29 (1) (2009) 1–16.
[22] chap. 13, ASHRAE Handbook Fundamental, American Society of Heating, Refrigerating and Air-Conditioning Engineers, SI-ed., Inc., Atlanta, 1993, pp. 14–15.
[23] ESDU 86018, Effectiveness-NTU Relations for the Design and Performance Evaluation of Two-Stream Heat Exchangers, Engineering Science Data Unit 86018 with Amendment, London ESDU International plc, 1991, pp. 92–107.
[24] J. Taborek, in: E.W. Schlünder (Ed.), Charts for Mean Temperature Difference in Industrial Heat Exchanger Configuration," Heat Exchanger Design Handbook, Hemisphere, Washington, DC, 1983. Chap. 1.5.
[25] V. Gnielinski, New equation for heat and mass transfer in turbulent pipe and channel flow, Int. Chem. Eng. 16 (1976) 359–368.
[26] K.A. Gardner, Efficient of extended surface, ASME Trans 67 (1945) 621.
[27] W.M. Kays, A. London, Compact Heat Exchangers, third ed., Mcgraw-Hill, New York, 1984.
[28] C.C. Wang, K.Y. Chi, C.J. Chang, Heat transfer and friction characteristics of plain fin-and-tube heat exchangers: Part II. Correlation, Int. J. Heat Mass Tran. 43 (15) (2000) 2693–2700.